SESA2022 Lab Report
Natalie Ko-Ferrigno 32748361

Abstract

In this laboratory report, various experimental, computational and theoretical methods are used to analyse the use of a NACA0020 airfoil for use in an aerial reconnaissance mission. The results from the different methods are compared, and recommendations are given for the airfoil.

1 Introduction

The airfoil laboratory was used to observe the pressure distribution over an infinite wing at various angles of attack. From the pressure distributions, the c_l and c_d could be calculated and compared against theoretical values from thin airfoil theory [5].

The finite wing laboratory was used to observe the effects of a 3 dimensional wing, as predicted by finite wing theory. By analysing this data, a comparison to the predictions from the airfoil laboratory could be drawn.

To classify the boundary layer of the airfoil, a laboratory was done on a thin plate to see how the boundary layer would behave at different Reynolds numbers. This was useful for estimating the skin friction coefficient, and therefore drag due to viscous effects. These effects would be present in the finite wing experiment, but not in the airfoil experiment.

Computational fluid dynamics was used to verify that the experimental results obtained are accurate. Operator error will likely play a smaller role, so they can be used as a rough baseline.

1.1 Aims and objectives

The aim of this laboratory is to assess the use of a NACA0020 airfoil in a UAV for monitoring a large geographical area.
- Data will need to be collected on each of the different methods
- This will then need appropriate handling and processing

2 Experimental and CFD methods

2.1 Airfoil laboratory

2.1.1 Method

For this laboratory, a NACA0020 airfoil of length $c = 0.063m$ was placed in an AF10 air flow bench, as shown in Figure 1. This airfoil had twelve pressure tappings, which were attached to an inclined manometer filled with dyed water. This manometer also had a total and static pressure readings, allowing the airspeed to be calculated. From this, the Reynolds number could be calculated with equation (1)[2].

$$Re = \frac{uc}{\nu} \tag{1}$$

The temperature was found through the thermometer on the flow bench, and the pressure was found through an online weather station [1]. From this, the density was found through the ideal gas law. This is shown in equation (2) [3].

$$\rho = \frac{v}{m} = \frac{p}{kT} \tag{2}$$

The speed of the flow was based on $Re_c = 100k$, which equates to about $25ms^{-1}$ and it was set by adjusting the dial on the bottom of the flow bench.

After setting the airspeed, the angle of attack could be set at various angles. After the angle of attack was set, the height of the liquid in each tube of the manometer was read off, and put into a Jupyter notebook to format the data and save it. After this, the airfoil was set to another angle of attack and the process was repeated. This process was done for every even angle of attack between $-4°$ and $14°$.

Figure 1: Air flow bench with manometer shown

2.1.2 Theory

Because the static and total pressures are measured, the freestream velocity can be found via equation (3). With the flow velocity, the actual Reynolds number experienced by the airfoil can be calculated to ensure dimensional accuracy.

$$U_\infty = \sqrt{\frac{2\left(p_{\text{total}} - p_{\text{static}}\right)}{\rho}} \tag{3}$$

Once U_∞ is known, the equation for pressure coefficients (as shown in equation 4) can be used to find the distribution of pressure along each surface. The difference between the surfaces can then be found, and this is the lift coefficient.

Because a NACA0020 airfoil has no camber, the lift curve slope should be $\frac{dc_l}{d\alpha} = 2\pi$ [5].

According to the Kutta condition [5], flow should leave the trailing edge of an airfoil smoothly, meaning at the same velocity from the upper and lower surfaces. This ensures that streamlines never cross, which is impossible. It can be used as an indication for how well an inviscid solver is working.

The pressure coefficient can take any value below 1, but if the pressure coefficient is higher than 1, there is an error in the measurement. Small errors may be down to the station measuring pressure being at a different altitude, but large errors will need more thorough investigation.

$$C_P = \frac{p - p_{\text{static}}}{\frac{1}{2}\rho U_\infty} \tag{4}$$

2.1.3 Potential sources of error

The pressure tappings do not extend all the way to the trailing edge. Because of this, the pressure data ends at $\frac{x}{c} = 0.794$. At the angles of attack measured, this could mean that some of the stall behaviour isn't measured.

The extrapolation of the data from the last measured point to the trailing edge will mean that the calculated coefficient of lift will be higher than it should be, as there will be a larger difference between the leading and trailing edges for longer.

The handle to control the speed of the flow was difficult to be precise with, as was the control for the angle of the airfoil in the airflow bench. Because of the short chord of the airfoil, small inaccuracies in the speed of the flow could lead to large inaccuracies in the Reynolds number. This would mean that important viscous effect may not be represented, and this could dramatically change the lift curve slope. As was mentioned previously, the actual Reynolds number can be measured.

With difficult angle adjustment, this could lead to a point in the lift curve slope being offset. This may not be evident if the error is small. This highlights the benefits of using a variety of methods. If the experimental data is significantly different to CFD methods, the experiment should be re-run to ensure that the error is accounted for. There is no way in the data measured to determine the actual angle the airfoil is at, so this relies on a well-executed experiment. To minimise the risk of this carrying an impact, the angle adjustment mechanism could use a lever in the future. This would make it more easy to make precise adjustments.

2.2 Boundary layer

2.2.1 Method

The equipment for this laboratory is almost identical to the experiment carried out in 2.1. The main change is that in place of a test foil section, there is a flat plate with a micrometer pitot tube.

For this experiment, boundary layers at multiple different boundary layers were observed. This was achieved by changing where the boundary layer is measured, and how fast the flow is going. The lowest Reynolds number used was 1×10^5, which is less than the transition number of 5×10^5 stated in [2]. However, because the flat plate may not be perfectly smooth, this could lead to the flow being turbulent.

After the test section shown in Figure 2 was attached to the airflow bench, the temperature was found by reading the thermometer on the airflow bench, and the pressure was found through online resources. The density could be found through equation 2. The distance of the plate from leading edge to pitot tube was found with a ruler. For the full length plate, this was expected to be $265mm$ and therefore $133mm$ for the half length plate. Then, the micrometer was zeroed. This involved visually taking the pitot probe to where it touched the wall with minimal force, taking care not to damage it. The reading on the micrometer was put into the Jupyter notebook.

Once these measurements of constants was done, the pitot tube was taken to about $10mm$ from the plate, which should be outside the boundary layer. To verify that the probe is outside the boundary layer, the micrometer was moved. Because the reading did not change, this was outside the boundary layer.

Once the probe was out of the boundary layer, it was moved inwards to some predetermined distances from the wall, ranging from $10mm$ of distance to $0.2mm$ of distance from the wall. More readings were done close to the wall in order to examine the viscous sub-layer. Once all the measurements were done for one Reynolds number, the flow speed was adjusted to change to the next Reynolds number to be measured, or the travelling pitot tube was moved to a different distance on the plate.

Figure 2: Air flow bench with flat plate shown

2.2.2 Theory

As stated before, the boundary layers of the plates will be turbulent given the Reynolds numbers. For this reason, turbulent boundary layer theory will be prioritised.

Because turbulent boundary layers are by definition unsteady, the pressure at the tip of the pitot tube is always fluctuating, meaning that a time averaged value is needed. This time averaged value is what will be calculated in 2.3. For a measuring device with a high temporal resolution, this could be achieved with an analog filter, or digitally. However, the inertia of a pitot tube means that the reading on the manometer is already time averaged.

One approximation of a turbulent boundary layer is given by equation 5. It states that the flow has no velocity at the wall, satisfying the no-slip condition [2], and the speed increases rapidly as a result of the eddies in the boundary layer leading to large amounts of mixing.

$$\frac{U}{U_\infty} = \left(\frac{y}{\delta}\right)^{\left(\frac{1}{n}\right)} \tag{5}$$

One definition of the boundary layer is where the local flow speed reaches $0.99U_\infty$ [2]. Because the free stream velocity is known, this can be interpolated. Through empirical observations, some links between Reynolds number and δ have been found. These are shown in equations 6. Because these are empirical observations, they should only be used to ensure the data is close to correct, rather than be a benchmark for a correct answer.

$$\frac{\delta_{\text{turb}}}{x} = \frac{0.38}{Re_x^{\frac{1}{5}}} \tag{6a}$$

$$\frac{\delta_{\text{lam}}}{x} = \frac{4.19}{\sqrt{Re_x}} \tag{6b}$$

There are also two more methods of quantifying the boundary layer that will be considered, the displacement thickness, as shown in equation 7, and momentum thickness, shown in 8.

$$\frac{\delta*}{\delta} = \int_0^\delta 1 - \frac{u}{U_\infty} d\frac{y}{\delta} \tag{7}$$

Displacement thickness is useful, because it shows the equivalent area a shape would need to have to represent the same drag in an inviscid flow.

$$\frac{\theta}{\delta} = \int_0^\delta \frac{u}{U_\infty} \left(1 - \frac{u}{U_\infty} \right) d\frac{y}{\delta} \qquad (8)$$

Momentum thickness can be used to represent the momentum of the fluid lost in the boundary layer, which is equivalent to drag from the plate caused up until that point. It can also be used to calculate the skin friction coefficient, which is the total drag on the surface. This is done via $C_F = \frac{2\theta(x=L)}{L}$

The shape factor is given by $H = \frac{\delta*}{\theta}$. If $H > 2$, the boundary layer is probably turbulent, and if $H < 2$, the boundary layer is probably laminar. This will be used to verify the assumption that all of the boundary layers are turbulent.

Blasius found that, when the curves were non-dimensionalised, different parts of the same boundary layer plotted on top of each other should look the same [2]. This can be used to show that the data collected is relevant and accurate.

When close to a wall, viscous effects can dominate. This leads to a new length scale based on the viscosity, from which velocity can be derived. These are y^+ and U^+. They are more useful in the section 2.3.

2.2.3 Potential sources of error

Due to the fact that other students have used the equipment, it is possible that the pitot tube has been damaged. This risk is minimised for the dataset used here by using reference data, however if that was not feasible, an alternative would be to check the data collected against the data other students had collected. This minimises the impact faulty equipment could have on the results.

Another potential source of error is misreading the manometer. This was counteracted by inclining the manometer to $60°$, which meant that any change in pressure lead to a larger change in the reading. This was corrected for in the Jupyter notebook.

It is possible that the equipment had been miscalibrated, such as a zero error on the micrometer, or the density of fluid in the manometer is incorrect. This is minimised through regular maintenance on equipment.

2.3 ANSYS Fluent

2.3.1 Method

A mesh of a NACA0020 airfoil was provided with inlets and outlets defined. There was plenty of space between the airfoil and the edges of the mesh so that the edges did not affect the performance of the airfoil. Upon launching Fluent, double precision was selected to make converging faster. The sst-k omega model was used. Temperature and pressure were matched to the lab conditions by changing ρ. In addition to this, many other settings were changed to be the same as the experimental conditions.

Then, the x and y components were set to have $U_\infty = 30ms^{-1}$ and α as desired. Turbulence intensity was set as 1% and 5% for the inlet and outlet respectively.

The reference area and length were set to $0.063m$. Under controls, momentum and pressure were set to 0.3. Report definitions were set up for lift and drag coefficients. All residuals were set to 1e-6. After initialisation, the calculation was run. Then, the mesh was refined where appropriate. Finally, the refined mesh was rerun.

For each level of refinement, the lift and drag coefficients were recorded from ANSYS, as were the $y+$ values and the pressure coefficients along the wing. Although the pressure coefficients weren't strictly necessary to obtain the lift and drag coefficients, it was useful for ensuring the algorithm used in 2.1 was accurate.

2.3.2 Theory

y^+ can be useful for CFD, because it should be under 1 across all of the mesh. This allows viscous effects to be captured.

Because ANSYS Fluent uses Reynolds Averaged Navier Stokes equations (RANS), it cannot accurately model turbulence. The outputs are time averaged, and the time average of an oscillation is 0, so every cell in the mesh is missing turbulence data. This is one of the limitations of RANS. However, it does greatly reduce the time to do a simulation, while not massively sacrificing accuracy.

2.3.3 Potential sources of error

In the export of a .xy file from ANSYS, there is no way to tell the upper surface from the bottom, potentially leading to errors in analysis with Python. These errors should be small, and as long as they are similar to the actual coefficients as reported by ANSYS, this shouldn't influence the results significantly.

2.4 Xfoil

2.4.1 Method

Xfoil direct analysis is opened through XFLR5, and a NACA0020 foil with 200 panels is imported. A type 1 analysis is defined, with a Reynolds number of $100k$. This is to match the boundary layer of the experiment. Then, a sequence is run, ranging from $-6°$ to $12°$. This is then exported for later analysis in Python.

2.4.2 Theory

Much of the theory for this section is covered in 2.1.2

It is well-documented that Xfoil can over-predict the lift-curve slope, and some attempts have been made to improve this [7]. This may lead to a steeper lift curve slope than is accurate.

2.5 Finite wing laboratory

2.5.1 Method

A NACA0012 airfoil was mounted in the 7x5 foot section of the R. J. Mitchell wind tunnel. The airfoil has a chord length of 0.4m and a span of 1.11m. The airfoil is connected to a stepper motor above, which controls the angle of attack. The stepper motor is finally connected to a force balance, which measures the force of the wing in 6 degrees of freedom. Each load cell in the force balance has an accuracy of $\pm 0.05N$.

Once the wing is mounted, the wind tunnel is turned on, and the speed in the test section is set to $20ms^{-1}$. Using the stepper motor to vary the angle of attack, the wing is moved from $-6°$ to $16°$ in increments of $1°$. The lift and drag are read from the force balance at each angle.

2.5.2 Theory

Due to the pressure difference across the airfoil, there is a tip at the edge. This causes downwash towards the tip, changing the angle of attack along the length of the wing. Because of this, the lift curve slope for a finite wing is always smaller than that of an infinite wing. To measure the difference between the lift curve slope of an airfoil and a finite wing, equation 9a can be used. a is the lift curve slope for the entire wing.

$$C_L = a(\alpha - \alpha_0) \tag{9a}$$

$$a = \frac{a_0}{1 + \frac{a_0}{\pi AR}(1 + \tau)} \tag{9b}$$

Because the wing is mounted to the wall at one end, there is only one tip vortex. This means that effectively half a wing is in the wind tunnel. Because of this, the span of the effective wing is 2.22m and each lift and drag force should be doubled.

The span efficiency factor as shown in 10a measures how much induced drag a wing produces. The closer to 0 it is, the better. There is also another value, the Oswald efficiency factor, that is derived from the span efficiency factor. This is shown in 10b.

$$\delta = \sum_{n=2}^{\infty} n \left(\frac{B_n}{B_1} \right)^2 \tag{10a}$$

$$e = \frac{1}{1 + \delta} \tag{10b}$$

2.6 XFLR5

2.6.1 Method

Through direct foil design, a NACA0012 airfoil was imported. 200 panels were used for increased precision. With Xfoil direct analysis, a batch analysis was run to determine the performance at a variety of Reynolds numbers. From this, the XFLR5 analysis could be run. The wing characteristics and Reynolds number were matched to that of section 2.5. The Lifting Line Theory analysis method was used. Then, the results were exported and analysed in Python. In addition to this, the lift distributions from some different angles of attack were also exported so that the lift distribution could be analysed.

2.6.2 Theory

XFLR5 has different analysis methods, but these will not be considered, because they weren't used. Documentation on the website [4] states that drag is underestimated in all analysis methods when compared to experimental results from a model sailplane. The analysis given states that lift is well-modelled for the LLT model.

As XFLR5 uses Xfoil to analyse airfoils, the lift over-prediction mentioned in Section 2.4.2 will also apply here.

Due to both of these effects, it is reasonable to assume that the glide ratio predicted by XFLR5 will be significantly different to that measured in section 2.5.

2.6.3 Potential sources of error

As with any unfamiliar software, a large potential source of error is incorrect usage. To combat this, the videos published on Blackboard have been used. It is also possible that the Python analysis is incorrect, however this has been tested against known examples to minimise the risk.

3 Results and discussions

3.1 Pressure distributions

It is clear that Xfoil is overpredicting pressure. This is particularly egregious in Figure 3c. On the other hand, ANSYS is underpredicting pressure. These trends are also visible on Figure 4.

Because of the limited number of pressure tappings on the experimental airfoil, it is clear that when $\frac{dc_p}{dx}$ is high, some data is lost. This will result in an underestimate of the lift coefficient.

On all the graphs, the ANSYS data has red bars going through the pressure distribution. This is because of the difficulties of reading the .xy file. At its worst, as shown in Figure 3a, this lead to a 16.4% error in the calculated lift coefficient. For most other values, this was less than 5%. Interestingly, for $\alpha = -2°$, the error was only 1.78%.

(a) Pressure distribution at $\alpha = 2°$ (b) Pressure distribution at $\alpha = 8°$ (c) Pressure distribution at $\alpha = 10°$
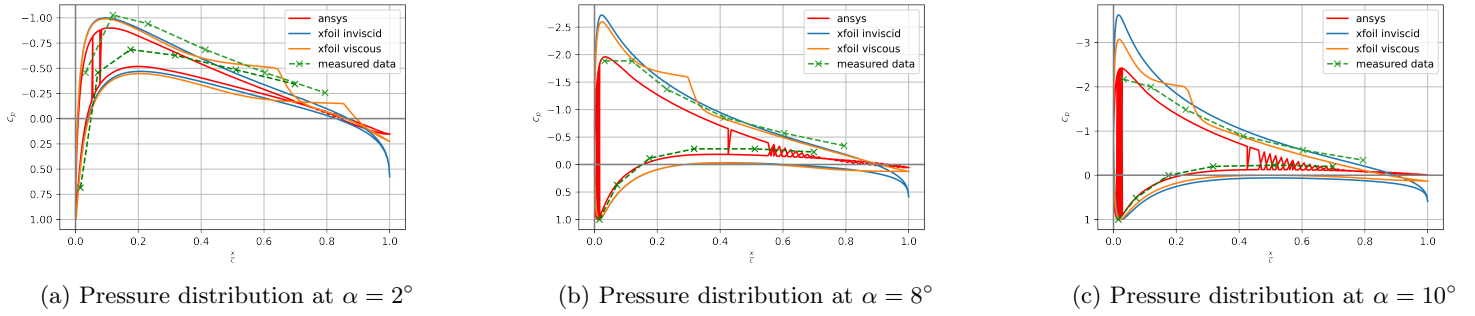
Figure 3: Pressure distributions across a NACA0020 airfoil, data collected through various means

3.2 Lift curve

As expected, Xfoil has overpredicted the lift. Because only the viscous pressure distributions are used, this is not overly significant. Using the large linear region from $-4°$ to $7°$ gave $\frac{dc_l}{d\alpha} = 8.35\text{rad}^{-1}$. The maximum predicted lift curve from thin airfoil theory is $2\pi = 6.28\text{rad}^{-1}$. This shows that, as stated in 3.1, Xfoil is overpredicting pressure.

The experimental data, as expected from the limited pressure tappings, underpredicted the lift coefficient. For the region $-4° \leq \alpha \leq 10°, \frac{dc_l}{d\alpha} = 5.00\text{rad}^{-1}$ To improve the accuracy of this, more tappings could be used. However, this is constrained by the geometry of the airfoil. The thin trailing edges mean that adding more tappings will be difficult without increasing the chord of the airfoil. An alternative solution is to use a digital force balance like is used in 2.5. This will massively increase accuracy, but will be extremely expensive for what appears to be marginal gain. Another error with the airfoil data is that ±2 should have the same magnitude, and the same with ±4. This may be a result of the location of the tappings not being symmetrical, meaning different parts of the pressure data were lost.

ANSYS has a lower $\frac{dc_l}{d\alpha}$ of 4.44rad^{-1}. This is expected, because of the thinner pressure distributions.

All of the methods of analysis seem to show the airfoil beginning stall at around $8°$. As α continues to increase, $\frac{dc_l}{d\alpha}$ is lower than before, as expected from section 2.1.2. A low y-intercept, and therefore lift at $\alpha = 0$, is also common to the fitted curves. The largest is only 0.004.

At $\alpha = 12$, the leading edge had a $c_p = 1.029$. This is usually indicative of an error, but in this case it may be due to external circumstances. According to their website, [1], the weather station used sits at an elevation of $32m$AMSL. Boldrewood Campus, where the airfoil experiment was carried out, sits at around $60m$ AMSL according to satelite observations [6]. This difference in ρ could explain this error. A solution would be a barometer in the same location as the experiment takes place.
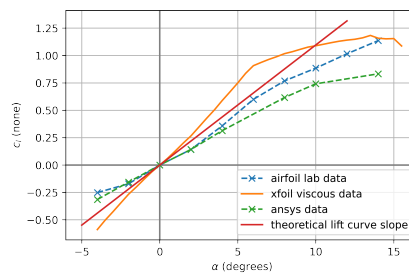
Figure 4: Comparison of the lift curve slopes of various 2 dimensional methods

Using equation 9b, the wing should have $a = 4.62\text{rad}^{-1}$ if it has an elliptic lift distribution, given its aspect ratio. This is shown on Figure 5

For XFLR, using the data $-6 \leq \alpha \leq 9$, a is found to be 4.64rad^{-1}. While this is higher than the theoretical value, this is probably because the Xfoil analysis gives lift curves that are higher than possible, and this issue continues into XFLR5. It also

has no body in the middle to disrupt the airflow, meaning that the lift distribution is more continuous. Stall occurs later than on the airfoil.

The measured data shows the effects of a constant-chord planform better. Because the lift distribution is not elliptic, $\tau \neq 0$. This decreases a to a value of 3.16rad^{-1}, meaning $\tau = 1.06$. a is lower than the theoretical value, probably because there is a boundary layer slowing down the flow half way through. In addition to this, there are no changes to planform or twist to make the lift distribution closer to being elliptic.
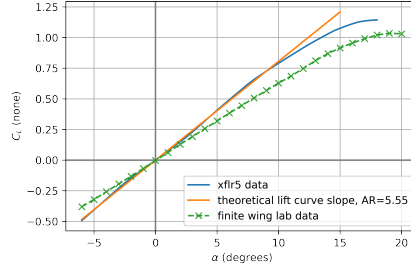
Figure 5: Comparison of the lift curve slopes of 3 dimensional methods

The effects of the lift being higher than realistic is visible in figure 6a, with the peak glide ratio being significantly higher. This can also be partially attributed to the underestimation of drag mentioned in 2.6.1. The magnitude of this is evident, as the maximum glide ratio is 9.76 for the real data and 23.35 for XFLR5.

It is clear in figure 6b that some of the data is incorrect. Because the NACA0020 airfoil is symetrical, $\alpha = -4$ should be $-\alpha = 4$. The calculated value of $c_d(\alpha = -4)$ is significantly higher than that for $\alpha = 4$, leading to the error. For the ANSYS figures, it appears something similar has happened and the value of c_d at $\alpha = 10$ is nearly $10\times$ higher than at $\alpha = 14$. This is likely down to user error, due to user unfamiliarity with the software.

ANSYS gave a maximum glide ratio of 33.31, Xfoil data gives it as 37.15 and the experimental data gives it as 13.64. The actual airfoil has significantly more surface roughness to the computational models, which may explain this.
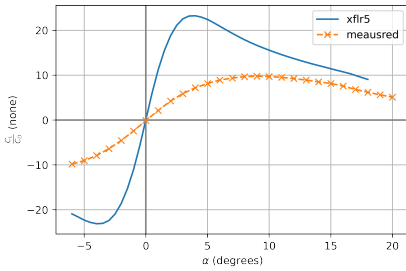
(a) Glide ratio for 3 dimensional methods
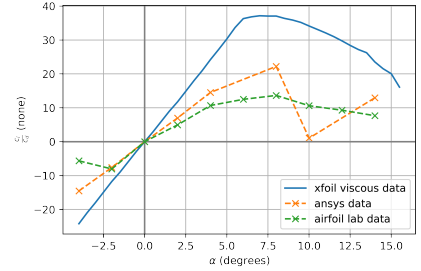
(b) Glide ratio for 3 dimensional methods

Figure 6: Glide ratios for airfoils and wings

The higher glide ratios for the airfoils is due to the wingtip vorticies present on the finite wing. These produce a lot of drag, hence the reduced aerodynamic efficiency.

3.3 Boundary layer laboratory

From Figure 7, it is clear that the turbulent profiles match the measured profiles better than laminar profiles do. This validates the assumption in 2.2.2. Table 3.3 shows the boundary layer thicknesses that are measured, as well as predicted by equation 6a. In addition, the shape factors show that all of the boundary layers are in fact turbulent.

	$Re_L = 400k$	$Re_L = 200k$	$Re_x = 200k$	$Re_x = 100k$
measured δ	$7.69mm$	$3.84mm$	$3.37mm$	$1.74mm$
using equation 6a	$7.63mm$	$8.77mm$	$4.38mm$	$5.03mm$
using equation 6b	$2.06mm$	$2.91mm$	$1.45mm$	$2.06mm$
shape factor	1.18	1.32	1.13	1.41

Becuase the Reynolds numbers are low for $Re_L = 200k$ and $Re_x = 100k$, the incorrect estimate for both laminar and turbulent may suggest that the pitot probe is very close to the transition. To verify this, more readings would need to be taken. It appears that for the other columns, equation 6a is close to accurate.
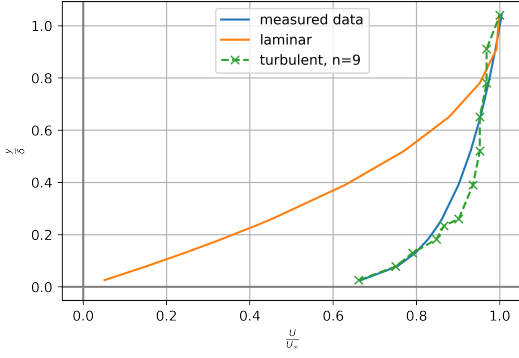
(a) Boundary layer at $Re_L = 400k$
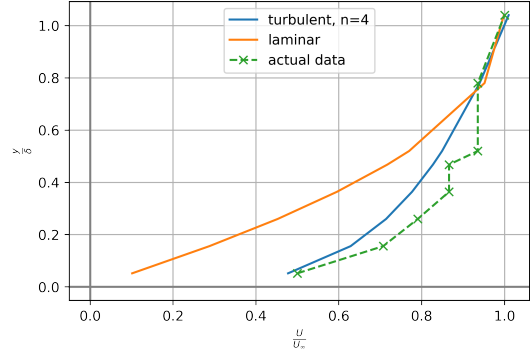
(b) Boundary layer at $Re_L = 200k$
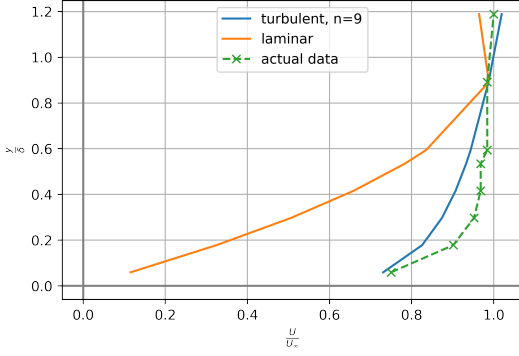
(c) Boundary layer at $Re_x = 200k$
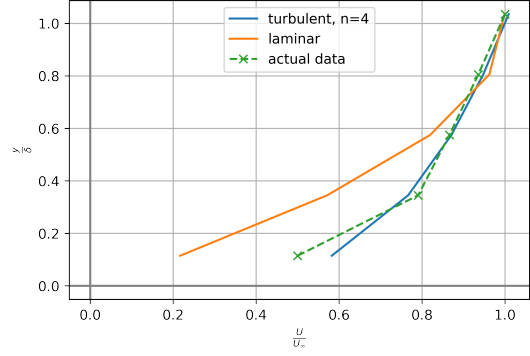
(d) Boundary layer at $Re_x = 100k$

Figure 7: Boundary layer profiles for all U_∞ and lengths tested

4 Conclusions

The NACA0020 is a good airfoil to begin with, with gentle stall characteristics and a reasonable glide ratio. Its issues include no lift at $\alpha = 0$, which may extend take-off distances, and other airfoils having better peak glide ratios. The first shortcoming could be solved either with a cambered airfoil, or by mounting a symmetric airfoil at an angle. To get a better glide ratio, the inverse design capabilities of Xfoil could be used.

When making the airfoil into a wing, a dual taper design will significantly decrease the amount of induced drag, making cruising more efficient. Having a high aspect ratio will also make the wing more efficient. Finally, mounting the wing in a parasol configuration will allow the lift distribution to be more continuous, making it yet more efficient.

A highly efficient aircraft is vital for surveying large areas of the Amazon raiforest for fires. The less power needed to continue flying, the further the aircraft can go.

References

[1] Southampton weather, 2023.

[2] J. Anderson. *Fundamentals of Aerodynamics*. McGraw-Hill Higher Education, NY, United States, 2016.

[3] J. Breithaupt. *AQA Physics A Level Student Book*. Oxford University Press, USA, 2016.

[4] A. Deperrois. Results vs prediction, 2019.

[5] M. Kaushik. *Thin Airfoil Theory*, pages 127–144. Springer Singapore, Singapore, 2019.

[6] C. Program. Eu-dem v1.1, 2017.

[7] G. Ramanujam and H. Ozdemir. *Improving Airfoil Lift Prediction*. 01 2017.